Electronic Supplementary Material (ESI) for ChemComm.

Supporting Information

Incorporating built-in electric field into NiFe LDH heterojunction for enhanced oxygen evolution and urea oxidation

Tianshan Song,[a] Hui Xue,[*a] Jing Sun,[a] Niankun Guo,[a] Jiawen Sun,[a] Yi-Ru Hao,[a] and Qin Wang[*a]

[a] College of Chemistry and Chemical Engineering, Inner Mongolia University, Hohhot 010021 (P. R. China)

*Corresponding authors: E-mail: qinwang@imu.edu.cn (Q. Wang)

1. Experimental

Materials

$Ni(NO_3)_2·6H_2O$ (98.0%), $Fe(NO_3)_3·9H_2O$ (99.0%), and $Co(NO_3)_2·6H_2O$ (99.5%) were all purchased from Tianjin Fengchuan chemical reagent technology Ltd. KOH (95.0%), 2-Methylimidazole (98.0%), Urea (99.0%), and RuO_2 (Ru>75.0%) was purchased from Aladdin. Deionized water was used to prepare all solutions.

Preparation of ZIF-67/CC

The carbon cloth (CC, 2 cm × 3 cm) was initially immersed in a concentrated nitric acid solution and subjected to hydrothermal treatment at 140 °C for 10 hours to achieve hydrophilic modification. The $Co(NO_3)_2·6H_2O$ (0.29 g) and 2-methylimidazole (0.66 g) were individually dissolved in 20 ml of deionized water, referred to as solution A and solution B respectively. Subsequently, solution A and solution B were swiftly mixed. The pre-exposed carbon cloth was immersed in the mixture and allowed to incubate for 5 hours at ambient temperature. The sample was subjected to triple rinsing with water and ethanol, followed by vacuum oven drying for 8 hours, resulting in the acquisition of ZIF-67/CC.

Preparation of Co-NC/CC

The synthesized ZIF-67/CC is placed in a ceramic boat and then inserted into a tube furnace. The temperature is raised to 800 °C with a heating rate of 5 °C min^{-1}, and maintained for 3 hours under a mixed atmosphere of H_2/Ar (5%/95%). The Co-NC/CC sample is subsequently obtained by allowing it to cool naturally to room temperature.

Preparation of NiFe LDH/CC

The counter electrodes were composed of carbon rods, while the reference electrodes consisted of Ag/AgCl (3 M), and pre-treated carbon cloth was utilized as the working electrode. The electrolyte was prepared by dissolving 0.129 g of $Ni(NO_3)_2 \cdot 6H_2O$ and 0.183 g of $Fe(NO_3)_3 \cdot 9H_2O$ in 50 mL of water. The electrodeposition process was conducted for a duration of 600 s using an electrochemical workstation, with a voltage applied at -1 V. Subsequently, the resulting NiFe LDH/CC catalyst was subjected to three rounds of rinsing with water and ethanol, followed by vacuum drying.

Preparation of Co-NC@NiFe LDH/CC

The Co-NC@NiFe LDH/CC was obtained through the electrodeposition of NiFe LDH onto the surface of Co-NC/CC in a three-electrode system. The counter electrodes were composed of carbon rods, the reference electrodes consisted of Ag/AgCl (3 M), and Co-NC was employed as the work electrode. The electrolyte was prepared by dissolving 0.129 g of $Ni(NO_3)_2 \cdot 6H_2O$ and 0.183 g of $Fe(NO_3)_3 \cdot 9H_2O$ in 50 mL of water. Electrodeposition was carried out for 600 s using an electrochemical workstation at a voltage of -1 V. Finally, the resulting catalyst was rinsed three times with water and ethanol and vacuum dried.

Preparation of RuO_2/CC

The 10 mg of RuO_2 was added to a mixed solution of 20 μL of Nafion (5%), 100 μL of anhydrous ethanol solution, and 880 μL of deionized water to form ink. Then, the 10 μL of ink were evenly spread on the CC (Geometric Area: 0.25 cm^2).

2. Material characterization

The crystalline phase structure of the catalysts was tested using an X-ray diffractometer. The model of the instrument was Rigaku Ultima IV. Scanning electron microscopy was used to study the morphology of the catalysts. The microstructure of the catalysts was investigated using a transmission electron microscope, and the spacing of the crystalline surfaces was investigated using a ZEISS Gemini 300. The instrument is an FEI Tecnai G2F 20. X-ray photoelectron spectroscopy was used to test the surface chemical composition and valence states of the catalysts. The instrument is an XSAM800 photoelectron spectrometer.

3. Electrochemical measurements

The electrochemical properties of catalysts were tested using Shanghai CHI760E electrochemical workstation. In the traditional three-electrode system, the carbon rod is the counter electrode, the Hg/HgO electrode is the reference electrode, and the obtained catalyst is the working electrode. The OER activity of the catalysts was tested using linear scanning voltammetry (LSV) in 1.0 M KOH solution at room temperature with a scan rate of 5 mV s^{-1} and corrected for the automatic iR compensation (90%). This has been provided in the supporting information.The double layer capacitance was tested using cyclic voltammetry (CV). The stability of the catalyst was assessed through timed-current (i-t) and cyclic voltammetry (CV). The UOR activity was tested using LSV in 1.0 M KOH and 0.5 M urea solution at room temperature with a scan rate of 5 mV s^{-1}. The stability of the catalyst was measured by cyclic voltammetry and chrono-potentiostatic (v-t). All potentials in the article have been converted to hydrogen electrode potentials (E_{RHE} = 0.059*pH +

$E^0_{(Hg/HgO)}$ + $E_{(Hg/HgO)}$). The Faraday yield is calculated from the total amount of oxygen produced (n_{O_2}: mmol) and the total amount of charge Q (C) passing through the cell. Suppose four electrons are required to produce O_2 molecule, the faradaic efficiency = 4F × $\frac{n_{O_2}}{Q}$= 4F ×n_{O_2}×10/t, where Q = t × 0.1 (C), F is the Faraday constant, and t represents the time (s) for the test time. The overall quantity of oxygen produced during the test is calculated by means of drainage.

4. Computational methods

We have employed the Vienna Ab Initio Package (VASP) [1,2] to perform all the density functional theory (DFT) calculations within the generalized gradient approximation (GGA) using the PBE [3] formulation. We have chosen the projected augmented wave (PAW) potentials [4,5] to describe the ionic cores and take valence electrons into account using a plane wave basis set with a kinetic energy cutoff of 450 eV. Partial occupancies of the Kohn-Sham orbitals were allowed using the Gaussian smearing method and a width of 0.05 eV. The electronic energy was considered self-consistent when the energy change was smaller than 10^{-5} eV. A geometry optimization was considered convergent when the force change was smaller than 0.05 eV/Å. Grimme's DFT-D3 methodology [6] was used to describe the dispersion interactions. During structural optimizations, the gamma point in the Brillouin zone was used for k-point sampling, and the bottom three atomic layers of part were fixed while the rest were allowed to relax. The free energy of a gas phase molecule or an adsorbate on the surface was calculated by the equation G = E + ZPE − TS, where E is the total energy, ZPE is the zero-point energy, T is the temperature in kelvin (298.15

K is set here), and S is the entropy. The reported standard hydrogen electrode (SHE) model [7] was adopted in the calculations of Gibbs free energy changes (ΔG) of all reaction steps, which was used to evaluate the reaction barrier.

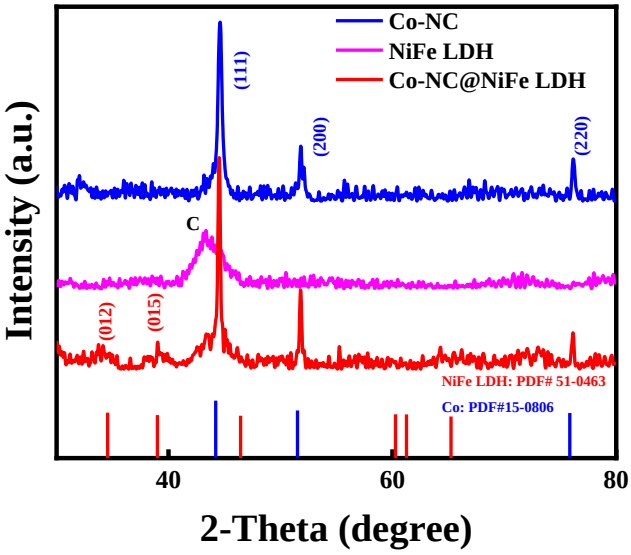

Fig. S1. XRD spectra of various samples.

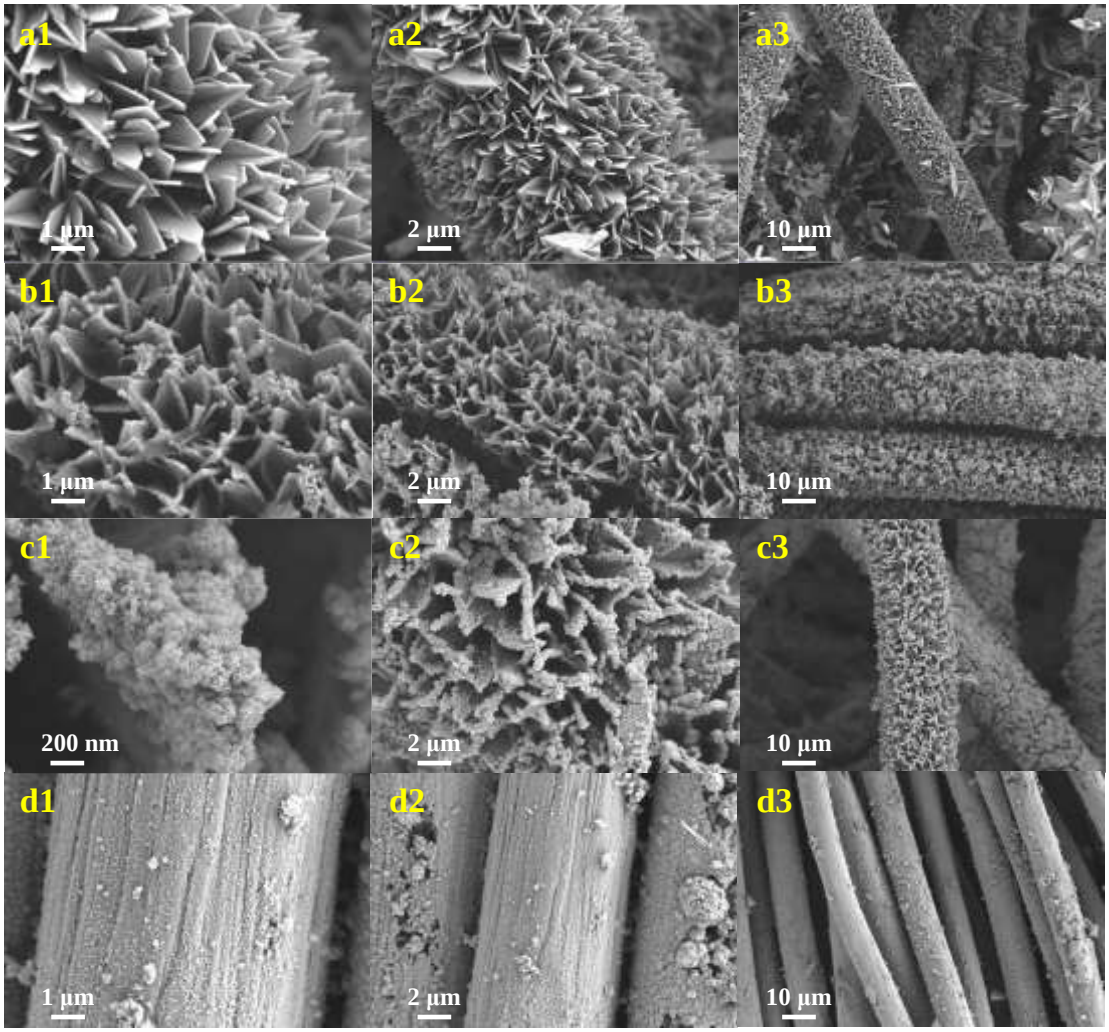

Fig. S2. SEM images of (a1-a3) ZIF-67, (b1-b3) Co-NC, (c1-c3) Co-NC@NiFe LDH, and (d1-d3) NiFe LDH.

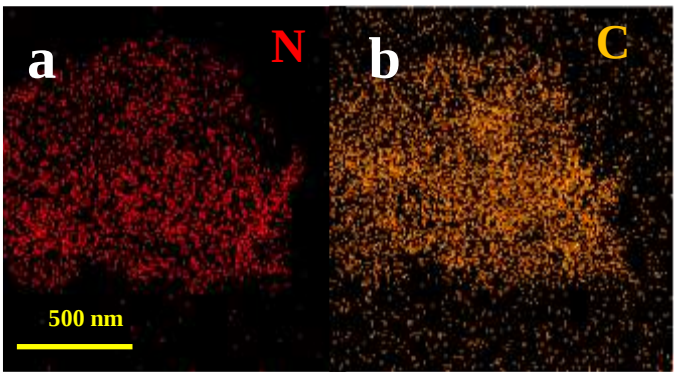

Fig. S3. N and C elemental mapping of Co-NC@NiFe LDH.

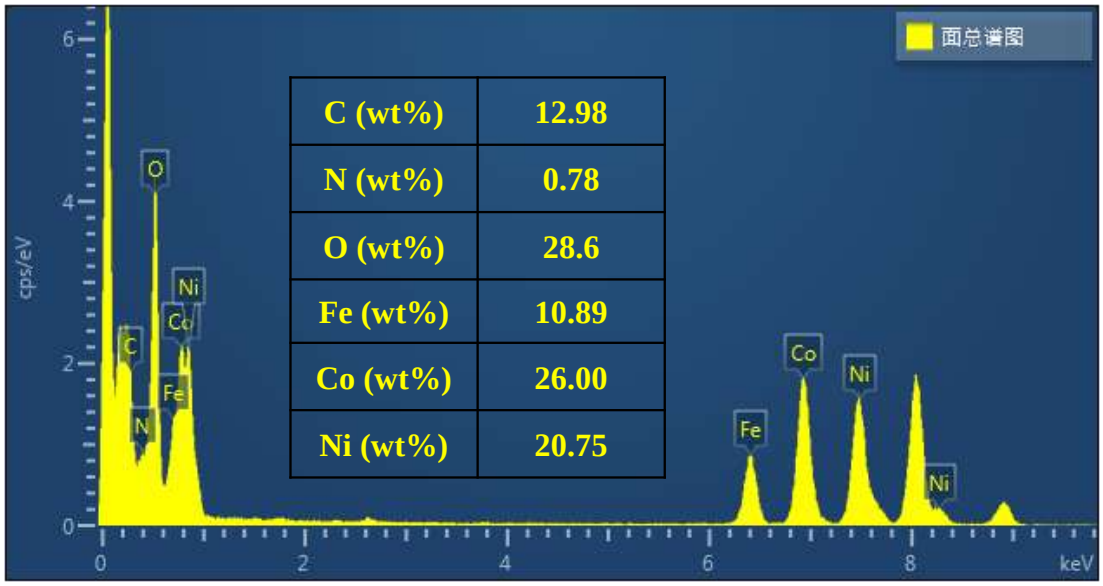

C (wt%)	12.98
N (wt%)	0.78
O (wt%)	28.6
Fe (wt%)	10.89
Co (wt%)	26.00
Ni (wt%)	20.75

Fig. S4. EDS spectrum of Co-NC@NiFe LDH.

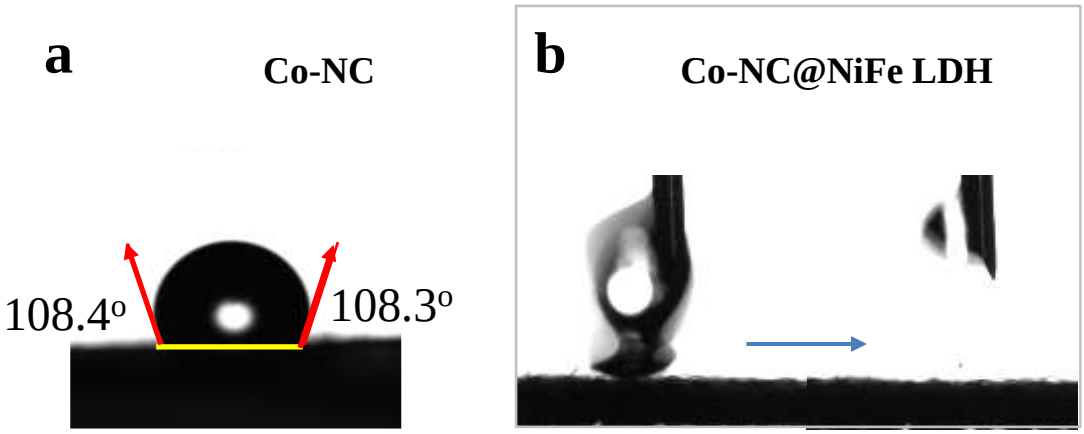

Fig. S5. Contact angle of (a) Co-NC and (b) Co-NC@NiFe LDH.

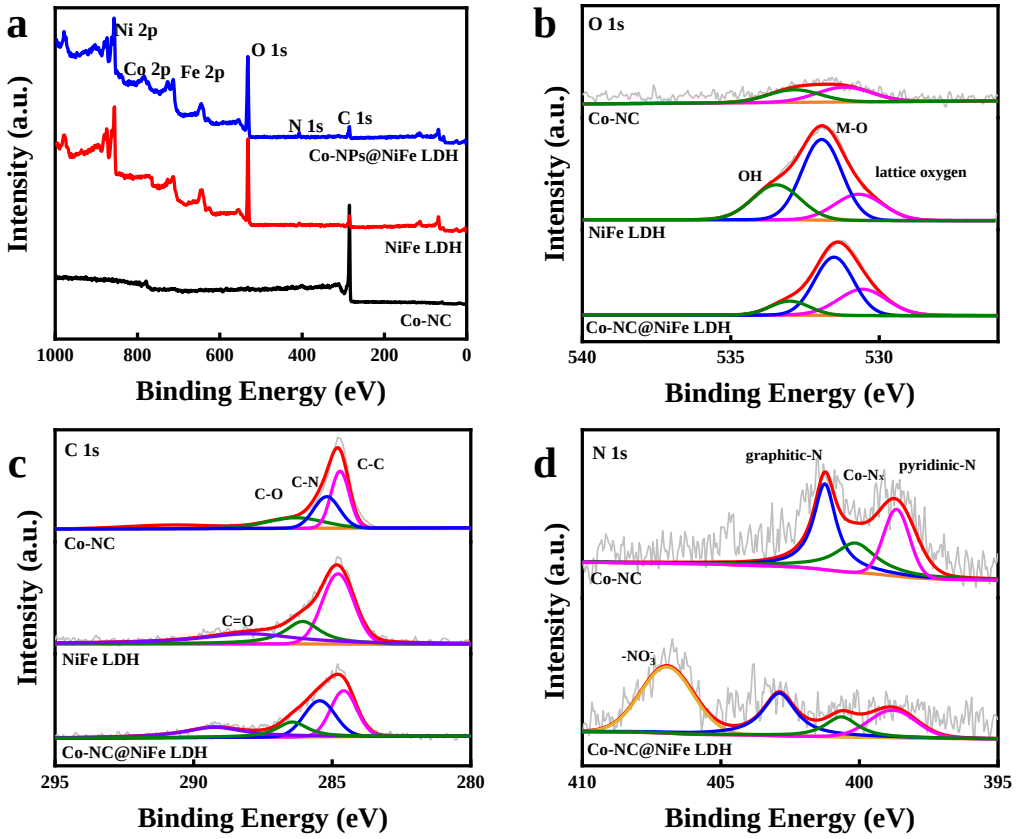

Fig. S6. XPS spectra of various samples (a) full spectrum, (b) O 1s, (c) C 1s, and (d) N 1s.

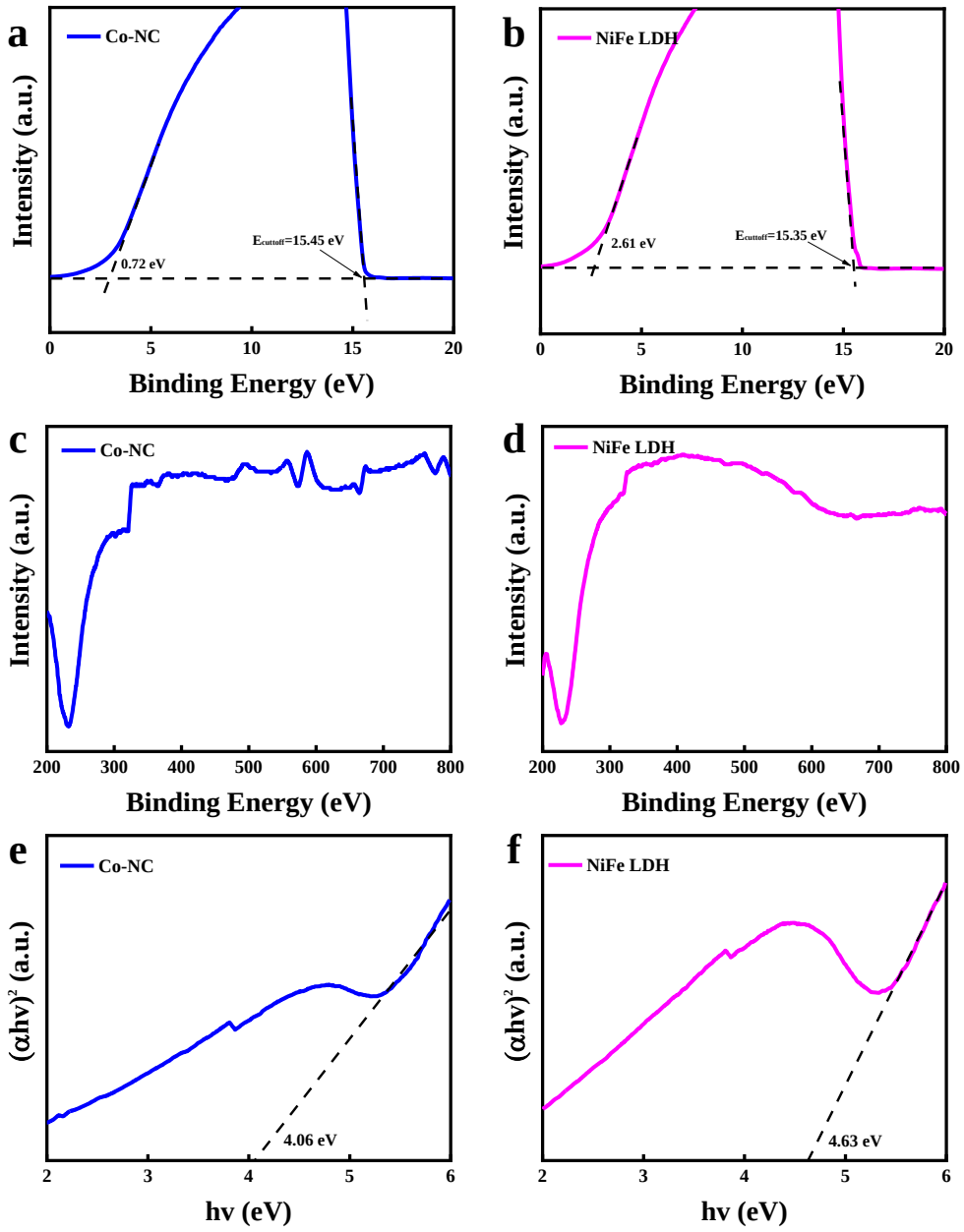

Fig. S7. UPS spectra of (a) Co-NC and (b) Co-NC@NiFe LDH. UV-vis spectra and corresponding the Tauc plots of the catalysts (c, e) Co-NC and (d, f) Co-NC@NiFe LDH.

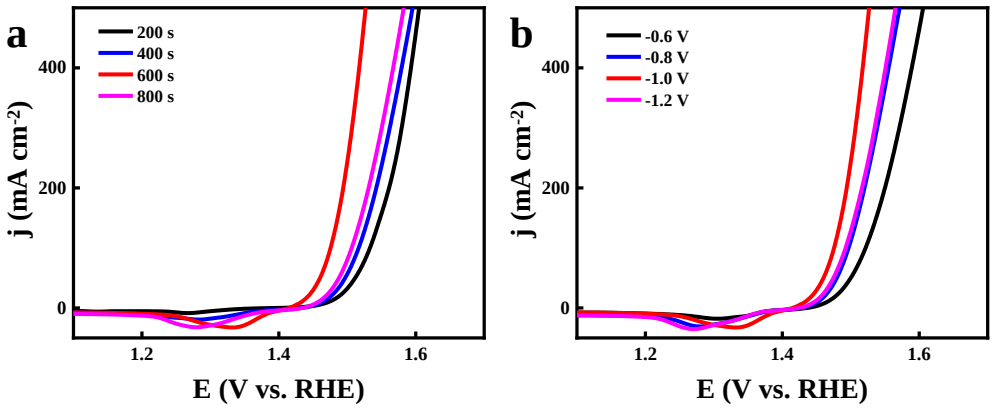

Fig. S8. OER polarization curves of catalysts prepared under different electrodeposition time and voltage.

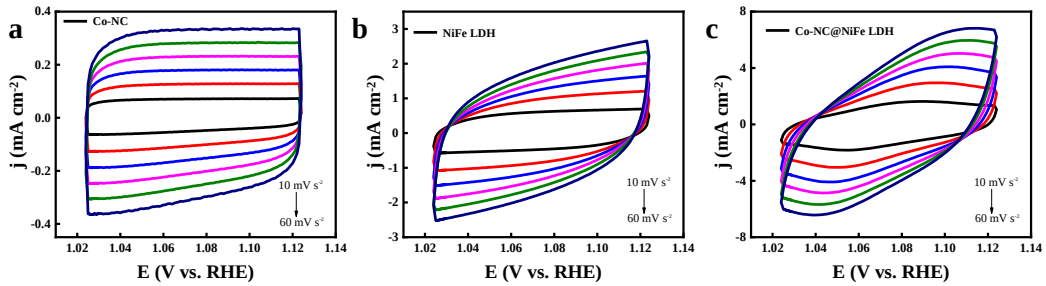

Fig. S9. CV curves under different scanning speeds of various samples (a) Co-NC, (b) NiFe LDH, and (c) Co-NC@NiFe LDH for OER.

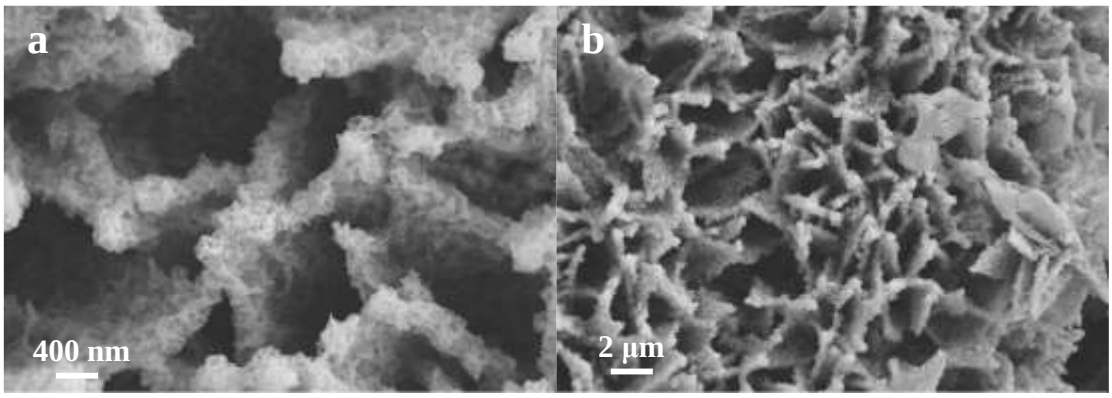

Fig. S10. SEM images of Co-NC@NiFe LDH after 2000 cycles test for OER.

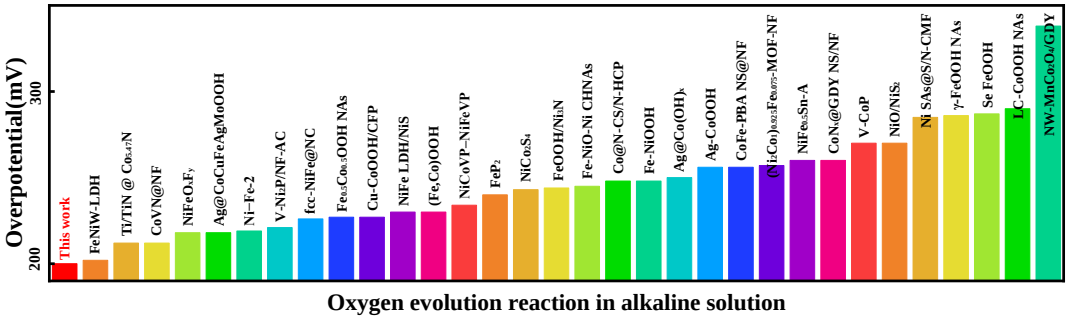

Fig. S11. Comparison of OER activity in recently reported catalysts.

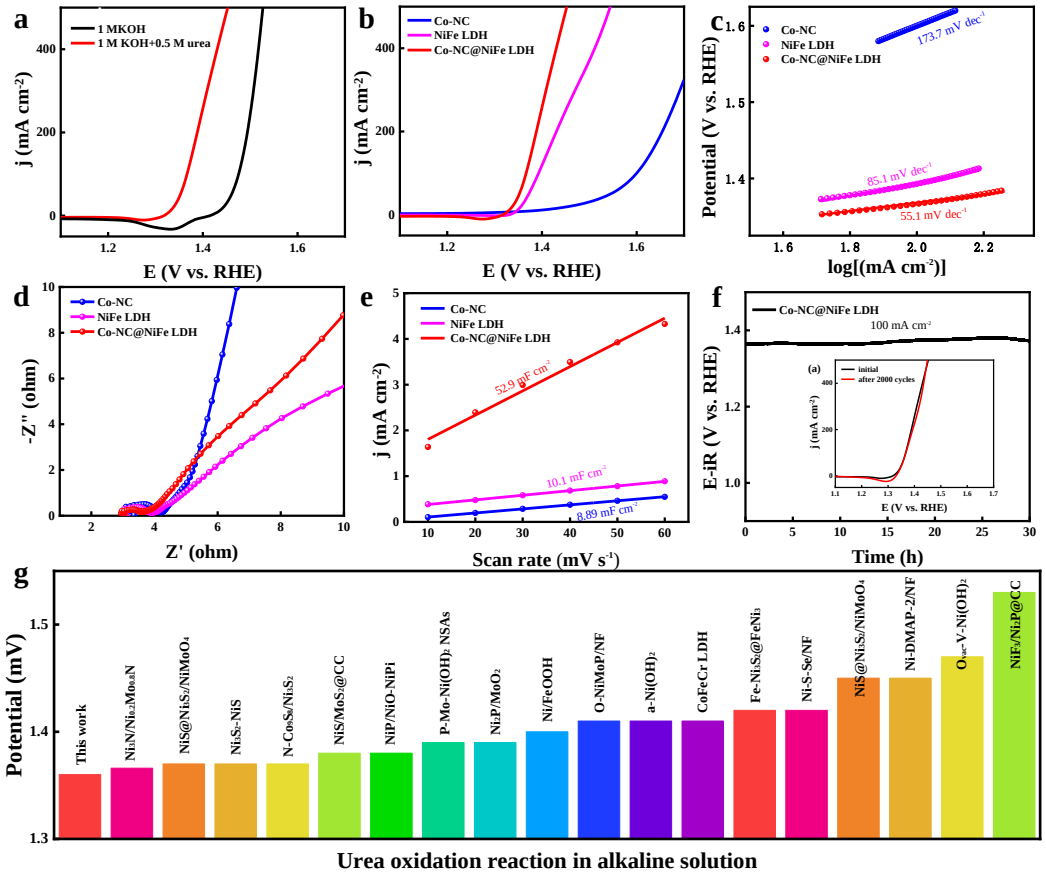

Fig. S12. UOR performances in 1.0 M KOH and 0.5 M urea. (a) The performance of Co-NC@NiFe LDH for UOR and OER in 1.0 M KOH solutions with and without 0.5 M urea, (b) UOR LSV curve, (c) Tafel plots, (d) EIS, (e) Cdl values, (f) chronopotentiometric tests of Co-NC@NiFe LDH (inset reveals the LSV curves of Co-NC@NiFe LDH before and after 2000 cycles), and (g) Comparison of UOR activity in recently reported catalysts.

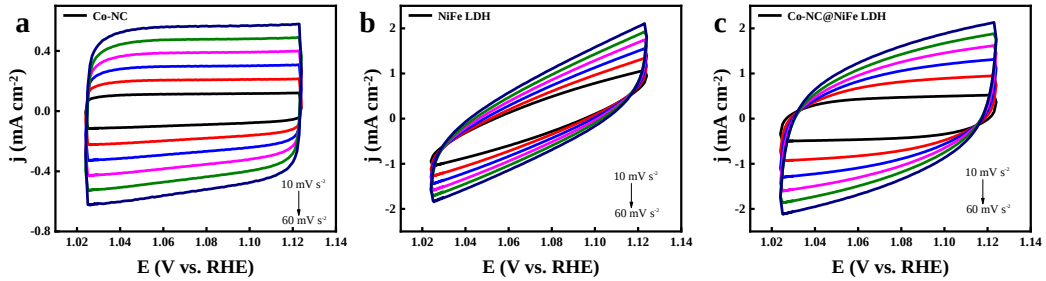

Fig. S13. CV curves under different scanning speeds of various samples (a) Co-NC, (b) NiFe LDH, and (c) Co-NC@NiFe LDH for UOR.

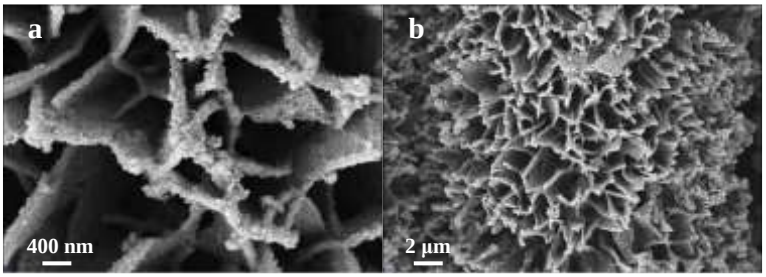

Fig. S14. SEM images of Co-NC@NiFe LDH after 2000 cycles test for UOR.

The UOR activity of the catalyst was further tested in an electrolyte containing 1.0 M KOH and 0.5 M urea. As depicted in Fig. S12a, the UOR potential at 100 mA cm^{-2} exhibits a reduction of 109 mV compared to the OER potential. The UOR overpotential of Co-NC@NiFe LDH is as low as 1.36 V, in comparison to the values of 1.6 V for Co-NC and 1.39 V for NiFe LDH (Fig. S12b). The Tafel slopes for Co-NC, NiFe LDH, and Co-NC@NiFe LDH were measured to be 173.7, 85.1, and 55.1 mV dec^{-1}, respectively. Notably, the Tafel slope of Co-NC@NiFe LDH exhibits the smallest value among all tested catalysts, indicating its superior kinetic performance in facilitating the reaction (Fig. S12c). The Co-NC@NiFe LDH catalyst exhibits a minimum impedance radius, as depicted in Fig. S12d, indicating that it possesses the lowest charge transfer resistance, which is consistent with the Tafel slope. From Fig. S12e and Fig. S13, the C_{dl} values of Co-NC, NiFe LDH, and Co-NC@NiFe LDH are 8.89, 10.1, and 52.9 mF cm^{-2}, respectively, providing evidence for the larger ECSA of Co-NC@NiFe LDH. The UOR stability of the Co-NC@NiFe LDH catalyst was assessed by measuring the timing potential and conducting cyclic voltammetry (CV) cycling. Fig. S12f shows that the overpotential of the catalyst remains relatively unchanged after a constant current test (100 mA cm^{-2}) for 30 hours. Furthermore, the LSV curves before and after the reaction remain essentially coincident even after 2000 CV cycles. The SEM analysis of the catalyst after stability testing reveals that the sheet array morphology remains unaltered (Fig. S14). The experimental results unequivocally demonstrate the exceptional stability in the UOR of Co-NC@NiFe LDH catalyst. As can be seen from Fig. S12g and Table S2, the UOR catalytic activity of Co-NC@NiFe LDH surpasses that of recently published non-noble metal catalysts.

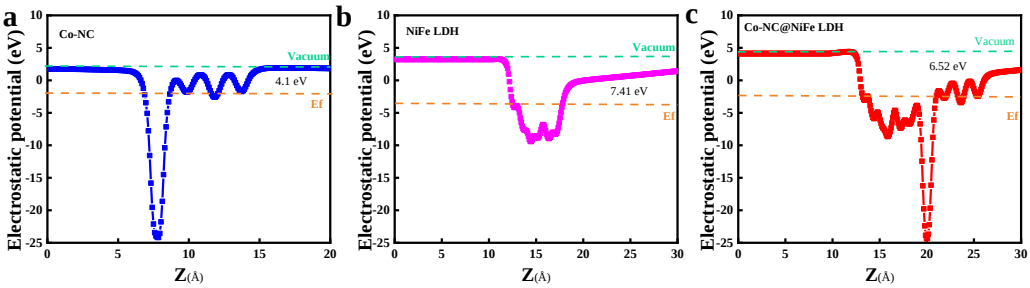

Fig. S15. Electrostatic potential distribution diagram.

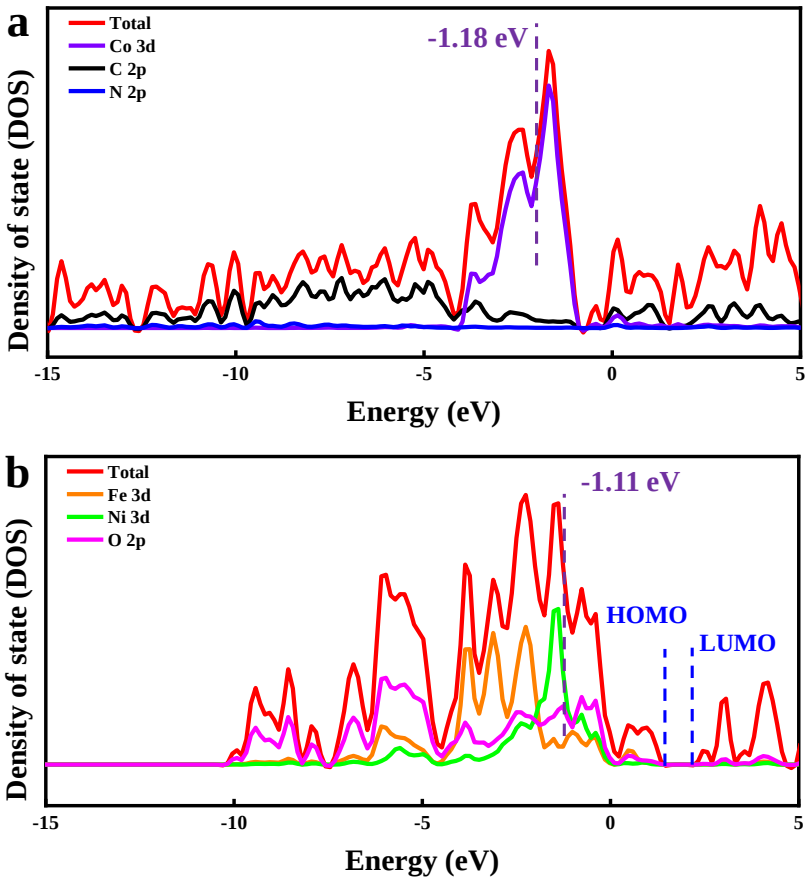

Fig. S16. Density of states corresponding to (a) Co-NC and (b) NiFe LDH.

Table S1. The atomic percentage of different elements in various catalysts.

Catalyst	C (at.%)	O (at.%)	N (at.%)	Co (at.%)	Fe (at.%)	Ni (at.%)
Co-NC	92.5	2.49	3.91	1.11	----	----
NiFe LDH	20.75	51.27	----	----	11.64	16.34
Co-NC@NiFe LDH	19.12	46.44	2.86	3.75	8.77	19.05

Table S2. Summary of representative catalysts that have been recently reported in an alkaline medium of OER.

Catalyst	η (mV)@j (mA cm^{-2})	Substrate	Reference
Co-NC@NiFe LDH	200@10	CC	This work
FeNiW-LDH	202@10	FF	*Nano Energy*, **2021**, 80, 105540
Ti/TiN@$Co_{5.47}N$	212@10	Ti foil	*Adv. Funct. Mater.*, **2021**, 31, 2008511
CoVN@NF	212@10	NF	*Adv. Energy Mater.*, **2020**, 2002464
$NiFeO_xF_y$	218@10	NF	*Nano Lett.*, **2021**, 21, 492-499
Ag@CoCuFeAgMoOOH	218@10	Cu foil	*Adv. Mater.*, **2022**, 34, 2110511
Ni−Fe-2	219@10	NF	*ACS Energy Lett.*, **2019**, 4, 622-628
V-Ni_2P/NF-AC	221@10	NF	*Adv. Funct. Mater.*, **2021**, 31, 2100614
fcc-NiFe@NC	226@10	CC	*Angew. Chem. Int. Ed.*, **2019**, 58, 6099-6103
$Fe_{0.5}Co_{0.5}$OOH NAs	227@10	CFC	*Appl. Catal. B Environ.*, **2022,** 304, 120986
Cu-CoOOH/CFP	227@10	CFP	*Chem. Eng. J.*, **2021**, 405, 126198
NiFe LDH/NiS	230@10	NF	*Adv. Energy Mater.*, **2021**, 2102353
(Fe, Co)OOH	230@10	NF	*Adv. Mater.*, **2022**, 34, 2200270
NiCoVP–NiFeVP	234@10	NF	*J. Mater. Chem. A*, **2021**, 9, 12203
FeP_2	240@10	NF	Adv. Funct. Mater., **2020**, 30, 1907791
$NiCo_2S_4$	243@10	NF	*Adv. Funct. Mater.*, **2019,** 29, 1807031
FeOOH/Ni_3N	244@10	CC	*Appl. Catal. B Environ.*, **2020,** 269, 118600
Fe-NiO-Ni CHNAs	245@10	CFC	*Appl. Catal. B Environ.*, **2021,** 285, 119809
Co@N-CS/N-HCP	248@10	CC	*Adv. Energy Mater.*, **2019**, 1803918
Fe-NiOOH	248@10	NF	*Cell Rep. Phys. Sci.*, **2020**, 18, 100241

Ag@Co(OH)$_x$	250@10	CC	*Angew. Chem. Int. Ed.*, **2020**, 132, 7312-7317
Ag-CoOOH	256@10	Ag foil	*ACS Catal.*, **2020**, 10, 562-569
CoFe-PBA NS@NF	256@10	NF	*Nano Energy*, **2020,** 68, 104371
$(Ni_2Co_1)_{0.925}Fe_{0.075}$-MOF -NF	257@10	NF	*Adv. Mater.*, **2019**, 31, 1901139
$NiFe_{0.5}Sn$-A	260@10	CC	Adv. Sci., **2020**, 7, 1903777
CoN_x@GDY NS/NF	260@10	NF	*Nano Energy,* **2019,** 59, 591-597
V-CoP	270@10	NF	*Adv. Energy Mater.*, **2021**, 2101758
NiO/NiS_2	270@10	CFP	*Angew. Chem.Int. Ed.*, **2022**, 61, e202207217
Ni SAs@S/N-CMF	285@10	CP	*Adv.Mater.*, **2022**, 34, 2203442
γ -FeOOH NAs	286@10	NF	*Adv. Mater.*, **2021**, 33, 2005587
Se FeOOH	287@10	IF	*J. Am. Chem. Soc.*, **2019**, 141, 7005-7013
LC-CoOOH NAs	290@10	CFC	*ACS Catal.*, **2021**, 11, 6104-6112
NW-$MnCo_2O_4$/GDY	338@10	CC	*Adv. Funct. Mater.*, **2021**, 2107179

Note: NF: Ni foam; FF: Fe foam; CC: carbon cloth; CFC: carbon fiber cloth; CP: carbon paper; CFP: carbon fiber paper.

Table S3. Summary of representative catalysts that have been recently reported in alkaline medium of UOR.

Catalyst	η (V)@j (mA cm^{-2})	Substrate	Reference
Co-NC@NiFe LDH	1.36@100	CC	This work
$Ni_3N/Ni_{0.2}Mo_{0.8}N$	1.366@100	NF	*Chem. Eng. J.*, **2021**, 409, 128240
$NiS@Ni_3S_2/NiMoO4$	1.37@10	NF	*J. Mater. Chem. A*, **2020**, 8, 18055
Ni_3S_2-NiS	1.37@100*	NF	*ACS Sustainable Chem. Eng.*, **2021**, 9, 15582-15590
N-Co_9S_8/Ni_3S_2	1.37@100	NF	*Small*, **2023**, 2207425
NiS/MoS_2@CC	1.38@100	CC	*Chem. Eng. J.*, **2022**, 443, 136321
NiP/NiO-NiPi	1.38@100*	NF	*Chem. Eng. J.*, **2021**, 425, 130514
P-Mo-$Ni(OH)_2$ NSAs	1.39@100	NF	*Appl. Catal. B*, **2020**, 260, 118154
Ni_2P/MoO_2	1.39@100*	NF	*Appl. Catal. B*, **2020**, 269, 118803
Ni/FeOOH	1.4@100	NF	*Chem. Commun.*, **2020**, 56, 14713
O-NiMoP/NF	1.41@100	NF	*Adv. Funct. Mater.*, **2021**, 31, 2104951
a-$Ni(OH)_2$	1.41@100	NF	*J. Mater. Chem. A*, **2019**, 7, 13577
CoFeCr LDH	1.41@100	NF	*Appl. Catal. B*, **2020**, 272, 118959
Fe-Ni_3S_2@$FeNi_3$	1.42@100*	NFF	*Chem. Eng. J.*, **2020**, 396, 125315
Ni-S-Se/NF	1.42@100	NF	*Nano Energy*, **2021**, 81, 105605
$NiS@Ni_3S_2/NiMoO_4$	1.45@100*	NF	*J. Mater. Chem. A*, **2020**, 8, 18055
Ni-DMAP-2/NF	1.45@100	NF	*Mater. Today Energy*, **2022**, 27, 101024
O_{vac}-V-$Ni(OH)_2$	1.47@100	NF	*Adv. Funct. Mater.*, **2023**, 33, 2209698
NiF_3/Ni_2P@CC	1.53@100*	CC	*Chem. Eng. J.*, **2022**, 427, 130865

Note: NF: Ni foam; FF: Fe foam; CC: carbon cloth; CFC: carbon fiber cloth; CP: carbon paper; CFP: carbon fiber paper; NFF: NiFe foam; * Value calculated from the curve shown in the reference.

References

1. Kresse, G.; Furthmüller, J. Efficiency of Ab-Initio Total Energy Calculations for Metals and Semiconductors Using a Plane-Wave Basis Set. Comput. Mater. Sci. 1996, 6, 15-50.

2. Kresse, G.; Furthmüller, J. Efficient Iterative Schemes for Ab Initio Total-Energy Calculations Using a Plane-Wave Basis Set. Phys. Rev. B 1996, 54, 11169-11186.

3. Perdew, J. P.; Burke, K.; Ernzerhof, M. Generalized Gradient Approximation Made Simple. Phys. Rev. Lett. 1996, 77, 3865-3868.

4. Kresse, G.; Joubert, D. From Ultrasoft Pseudopotentials to the Projector Augmented-Wave Method. Phys. Rev. B 1999, 59, 1758-1775.

5. Blöchl, P. E. Projector Augmented-Wave Method. Phys. Rev. B 1994, 50, 17953-17979.

6. Grimme, S.; Antony, J.; Ehrlich, S.; Krieg, H. J. Chem. Phys. 2010, 132, 154104.

7. Nørskov, J. K.; Rossmeisl, J.; Logadottir, A.; et al. J. Phys. Chem. B 2004, 108, 17886-17892.